Journal of Thermal Analysis and Calorimetry (2020) 142:63–73
https://doi.org/10.1007/s10973-020-09522-0

Thermal cycling effect on the kinetics of glass transition and crystallization of a Zr-based bulk metallic glass

Pan Gong[1,2] · Fangwei Li[1] · Geng Yin[1] · Lei Deng[1] · Xinyun Wang[1] · Junsong Jin[1]

Received: 25 July 2019 / Accepted: 6 March 2020 / Published online: 16 March 2020

Abstract
We investigated the effects of thermal cycling on the kinetics of glass transition and crystallization of a classic Zr-based BMG (Vit-1) by differential scanning calorimetry (DSC). Two different thermal cycling conditions with different cycles and holding times were used. Sub–sub-T_g isothermal annealing condition was also adopted for comparison. Continuous DSC tests were conducted to calculate the activation energies of glass transition and crystallization based on different equations. Isothermal DSC tests were also conducted to further study the crystallization mechanisms in views of local Avrami exponent. Based on the experimental results, the related mechanisms have also been discussed.

Keywords Bulk metallic glasses · Thermal cycling · Kinetics · Glass transition · Crystallization · Structural relaxation

Introduction

Bulk metallic glasses (BMGs) are very attractive as potential advanced materials because of their unique physical and chemical properties [1, 2]. Thus, BMGs have been regarded as potential structural materials in many areas including aircraft, automobiles, cell phone parts, military equipment, medical devices, and sports apparatus. As BMGs are a class of metastable materials, for the structural application, the stability of structure and properties of BMGs in service should be taken into consideration. In the past years, the effects of many service conditions (such as fatigue load [3], impact load [4], corrosive environment [5], friction [6], and low/high temperature [7, 8]) on the structure and properties of BMGs have been studied.

Some structural parts, such as the gas turbine components, may suffer severe thermal cycling in service, which probably affects the structural and properties of metals and alloys including BMGs [9–13]. However, the research of thermal cycling effect on the properties of BMGs was seldom reported. Wang et al. studied the effect of thermal cycling on the structure and mechanical properties of Vit 1 [12] and Ti–Zr–Be–Al [13] BMGs with a temperature variation between − 196 and 150 °C. According to their results, after at least 200 cycles, the BMG samples still possess amorphous structure and no obvious change in mechanical properties has been observed. Wang et al's primary research is a meaningful effort, but further detailed work is still needed.

For BMGs, it is necessary to understand the kinetics of glass transition which is important to determine the thermal stability and glass transition behavior [14]. Scholars have studied the kinetics of glass transition of lots of BMGs such as Zr–Al–Ni [15], La–Al–Co [16], Ce–Al–Co [17], Ti–Cu–Ni [14], and Fe–Co–B–Si [14]. As BMGs are metastable materials, the crystallization kinetics should also be investigated to avoid crystallization [18–21]. There are some reports about the influence of sub-T_g and sub–sub-T_g annealing on the glass transition and crystallization behaviors of BMGs [22–24]. In this study, we systematically investigate the thermal cycling effect on the kinetics of glass transition and crystallization of BMGs by differential scanning calorimetry. Vit 1 alloy, which is a classic BMG developed

✉ Xinyun Wang
wangxy_hust@hust.edu.cn

✉ Junsong Jin
jsjin@hust.edu.cn

1 State Key Laboratory of Materials Processing and Die and Mould Technology, Huazhong University of Science and Technology, 1037 Luoyu Road, Wuhan 430074, Hubei, China

2 State Key Laboratory of Advanced Design and Manufacturing for Vehicle Body, Hunan University, Changsha 410082, Hunan, China

by Johnson's group [25], has been selected as the model material. Our work is meaningful to fully understand the glass transition behavior and rationally evaluate the service performance of BMGs.

Experimental procedure

The master Vit 1 ingots were prepared by arc melting under the protection of high-purity (99.995 mass%) Ar gas. High-purity (> 99.9 mass%) Zr bars, Ti bars, Cu plates, Ni plates, and Be pieces were used for preparing the ingots. Each ingot was about 20 g and remelted with the help of electromagnetic stirring for five times to ensure chemical homogeneity. Then, as-cast rods (3 mm in diameter and 55 mm in length) were prepared by copper mold suction casting. Thermal cycling treatment and annealing were conducted by DSC (Perkin Elmer Instruments, PYRI diamond). Figure 1 shows the schematic of thermal cycling and isothermal annealing. Thermal cycling was conducted in two different types denoted by type 1 and type 2, respectively. The former type consisted of 50 cycles, and each cycle had a heating time of 1.6 min, an annealing temperature of 533 K (sub–sub-T_g annealing), a hold time of 1 h, and a cooling time of 1.6 min on average. In "type 2" testing, there were 25 cycles and each cycle had the same heating time, annealing temperature, and cooling time as those of "type 1" testing. However, the hold time is 2 h, which is twice as that of "type 1" testing. For both the two types, the total holding times at 533 K during diffusion annealing were the same and counted. For comparison, another group of samples were isothermally annealed at a stable temperature of 533 K for 50 h. X-ray diffraction (XRD, Rigaku D/max-RB with Cu Kα radiation) was adopted to examine the structure of the as-cast- and thermal-treated samples. Continuous DSC tests of the as-cast- and thermal-treated samples were characterized using a NETZSCH STA 409 C/CD DSC (gas for protection: Ar) at four different heating rates (5, 10, 20, and 40 K min^{-1}). Isothermal DSC tests were conducted using DSC (Perkin Elmer Instruments, PYRI diamond). The samples with a mass of 20 mg were put in Al pan, heated to the desired temperature at a heating rate of 150 K min^{-1}, and then held until the crystallization process completed. In and Zr standards were used for the calibration, and the accuracies for the temperature and enthalpy are ± 0.2 K and ± 0.5 J g^{-1}, respectively.

Results and discussion

Figure 2 shows the XRD patterns of the samples experienced different heat treatments. All the spectra exhibit typical characterization of amorphous structure. Compared with the as-cast sample, the XRD patterns of the thermal-treated samples do not show significant difference, which confirms the structural stability of Vit 1 BMG upon the selected thermal treatments.

Figure 3 shows the continuous DSC curves of the as-cast- and thermal-treated Vit-1 samples at various heating rates ranging from 5 to 40 K min^{-1}. For all the samples, a strong dependence between the glass transition/crystallization and the heating rate during continuous heating process can be observed. Three exothermic events are observed after the glass transition process, implying a complex multi-step crystallization. These phenomena have been reported in some previous researches [26, 27]. Hays et al. [28] acclaimed that the first exothermic peak is related to the phase separation and primary crystallization, while the second exothermic peak can be attributed to a second crystallization process during which a more stable crystallization phase forms. With the increase of heating rate, the first and second

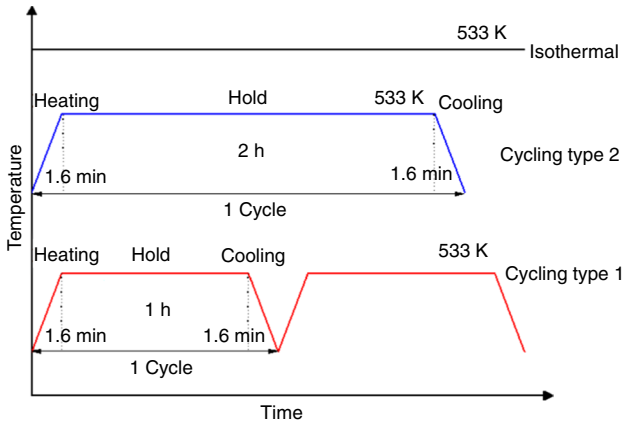

Fig. 1 Schematics of thermal cycling and isothermal treatment conditions for Vit-1 BMG

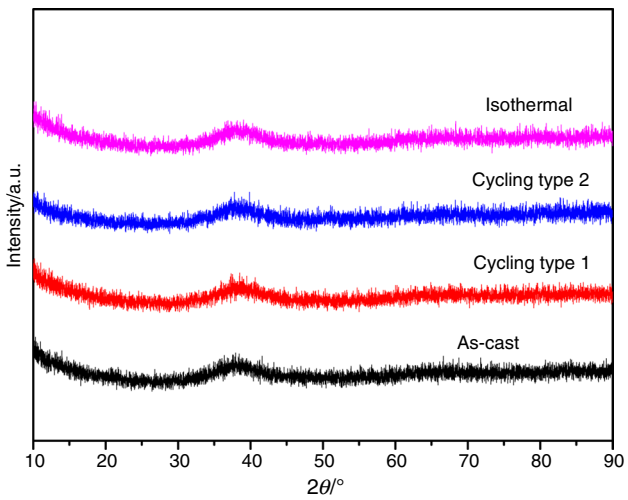

Fig. 2 XRD patterns of the as-cast- and thermal-treated Vit-1 samples

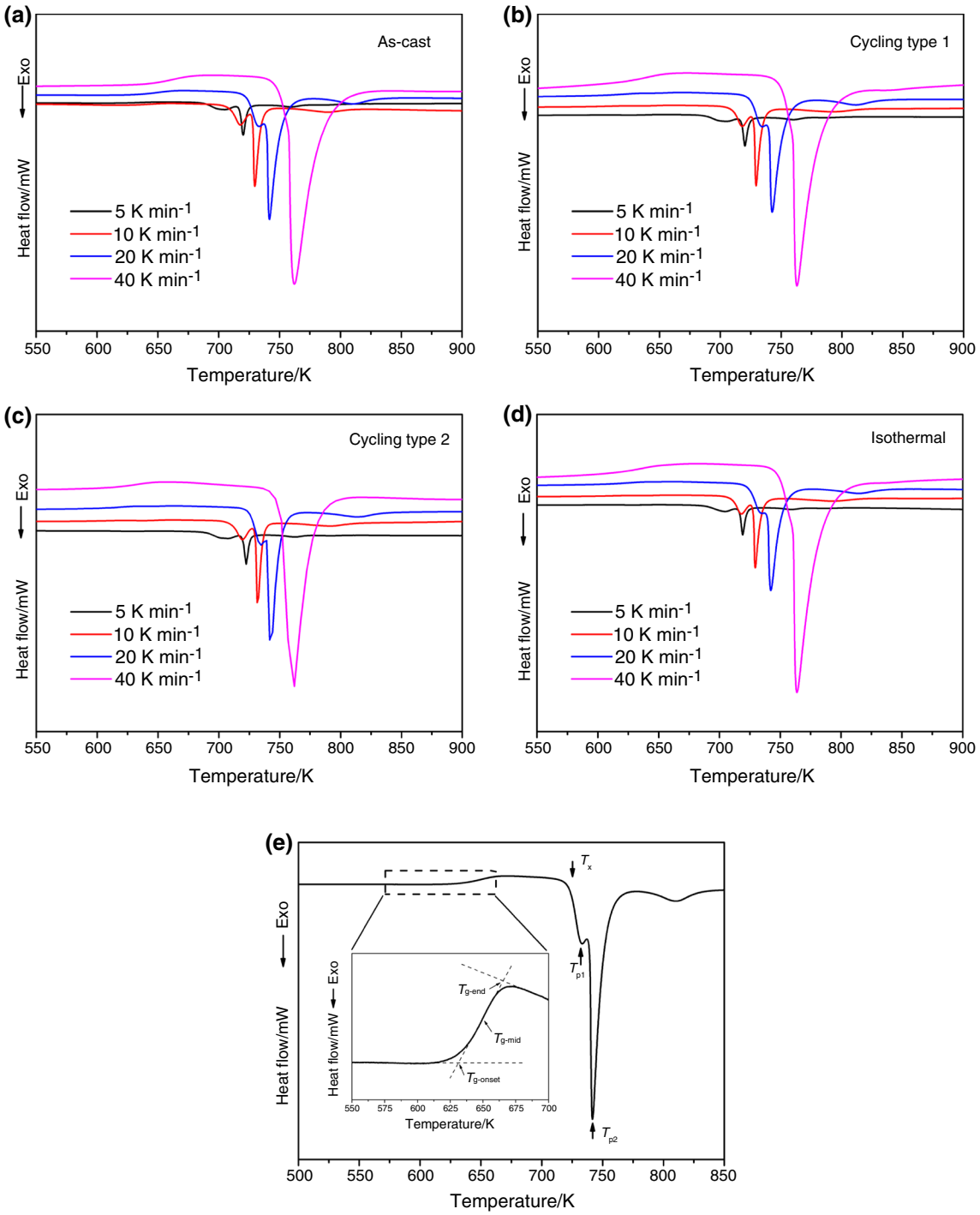

Fig. 3 Continuous DSC curves of the as-cast- and thermal-treated Vit-1 samples: **a** as-cast, **b** cycling type 1, **c** cycling type 2, and **d** isothermal annealing. **e** Shows the determination of T_g, $T_{p1,}$ and T_{p2} together with the different assignments of the glass transition temperature (T_g)

crystallization peaks merge gradually and forms one peak when the heating rate reaches 40 K min^{-1}.

In this study, three definitions for T_g were adopted (as shown in Fig. 3e). The black arrows also indicate the onset temperature of crystallization T_x and the temperatures corresponding to three crystallization peaks (T_{p1} and T_{p2}). Table 1 summarizes the values of the characteristic temperatures. As shown in Fig. 3 and Table 1, compared with the as-cast sample, the thermal-treated samples possess similar values of T_x, T_{p1}, and T_{p2} but much lower values of T_g. The thermal cycled type 2 sample exhibits the lowest value of T_g and the largest value of ΔT_x among the thermal-treated samples.

Table 1 Thermal properties of the as-cast- and thermal-treated Vit-1 samples

Sample	Heating rate/K min^{-1}	$T_{g\text{-onset}}$/K	$T_{g\text{-mid}}$/K	$T_{g\text{-end}}$/K	T_x/K	ΔT_x/K	T_{p1}/K	T_{p2}/K
As-cast	5	619.6	634.6	649.6	688.0	68.4	704.9	720.1
	10	626.6	641.9	657.2	708.2	81.6	717.9	729.7
	20	633.4	648.6	663.8	723.1	89.7	733.3	741.7
	40	640.5	662.4	684.2	747.6	107.1	–	762.2
Cycling type 1	5	553.7	580.9	608.1	687.4	133.7	705.2	720.2
	10	572.6	598.1	623.6	709.0	136.4	718.1	729.4
	20	593.8	613.6	633.4	723.5	129.7	734.5	742.5
	40	615.5	636.6	657.6	749.1	133.6	–	763.0
Cycling type 2	5	547.4	577.2	606.9	689.0	141.6	706.3	722.3
	10	568.1	594.2	620.3	709.5	141.4	719.3	731.2
	20	589.0	610.3	631.6	725.4	136.4	734.7	741.7
	40	604.7	629.6	654.5	750.1	145.4	–	762.0
Isothermal	5	560.8	586.4	612.0	687.8	127.0	704.8	719.1
	10	575.6	599.1	623.6	709.0	132.4	718.1	729.5
	20	594.1	621.6	649.1	723.9	129.8	734.9	742.3
	40	608.3	635.4	662.4	749.9	141.6	–	763.8

It can also be found that the supercooled liquid region ΔT_x (defined as $T_x - T_{g\text{-onset}}$) for the as-cast sample becomes wider with increase in heating rate. However, for the thermal cycled samples and the annealed sample, no obvious relationship between ΔT_x and heating rate can be observed.

The relationship between T_g and the heating rate ϕ follows the classic Lasocka relationship [29]:

$$T_g = A + B \ln \phi \tag{1}$$

where A denotes the glass transition temperature (heating rate: 1 K min^{-1}). B represents the response of the configuration changes within the glass transition region. Figure 4 shows the plots of T_g versus ln ϕ for the as-cast, thermal cycled, and annealed Vit-1 BMG samples. The obtained values of A and B are provided in Table 2. The values of B for the thermal-treated samples are found to be different from those for the as-cast sample, indicating that the thermal-treated samples undergo structural changes in varying degrees. The thermal cycled type 1 sample exhibits the largest value of B, and this may relate to the largest degree of structural relaxation. However, as the T_g of the thermal-treated samples still follows Lasocka's relationship, the kinetics nature of the glass transition for the Vit-1 BMG does not change by the thermal cycling and isothermal annealing.

Moynihan method and Kissinger method were adopted to calculate the activation energies of glass transition. The Moynihan equation can be written as [30]:

$$\ln \phi = -\frac{E}{RT} + \text{const.} \tag{2}$$

The Kissinger equation can be written as [31]:

$$\ln\left(\frac{\phi}{T^2}\right) = -\frac{E}{RT} + \text{const.} \tag{3}$$

where ϕ denotes the heating rate, R is the gas constant (8.314 J mol^{-1} K^{-1}), and E and T represent the activation energy of glass transition and the glass transition temperature, respectively. The related Moynihan plots and Kissinger plots are shown in Figs. 5 and 6, respectively. Table 2 lists the calculated values of E_g. For all the four studied samples, a similar trend is found that the value of $E_{g\text{-end}}$ is the largest and the value of $E_{g\text{-onset}}$ is the lowest. By comparison, the values of E_g for the as-cast sample are the largest. The isothermal annealed sample comes second. The values of E_g for the thermal cycled samples are obviously lower, and the thermal cycled type 2 sample possesses the lowest values of E_g. The above results confirmed that thermal cycling has a great effect on the glass transition of Vit-1 BMG.

Kissinger method and Ozawa method are adopted to determine the activation energies for different crystallization events. The precondition of Kissinger method for calculating the activation energies of crystallization is the crystallized fraction corresponding to the characteristic temperatures which do not change a lot upon different heating rates. The latter considers the change in crystallized fraction during the crystallization process and reduced the calculation error, which can be expressed as [32]:

$$\ln(\phi) = -1.052\frac{E}{RT} + \text{const.} \tag{4}$$

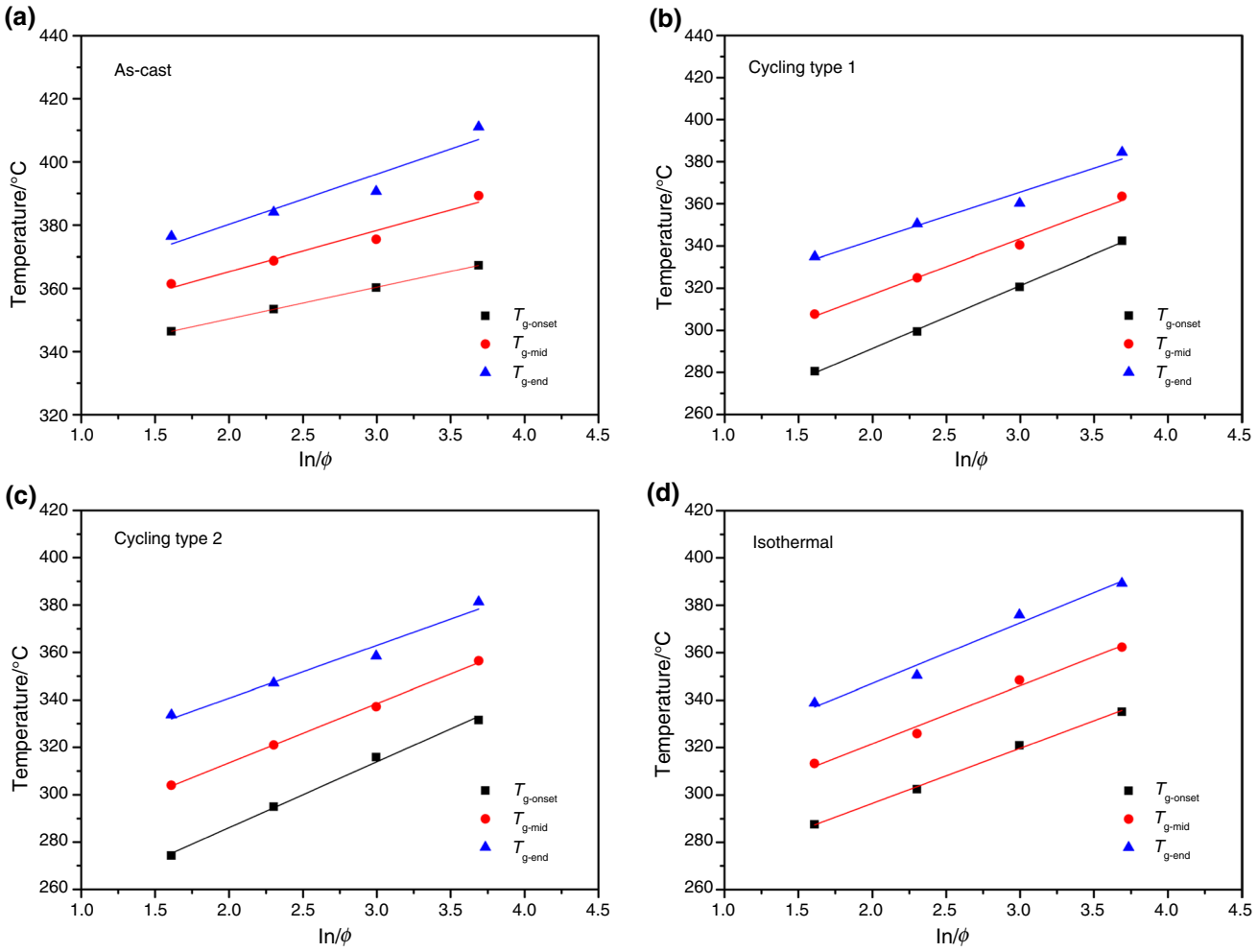

Fig. 4 Dependence of T_g with ln (ϕ) for **a** as-cast, **b** cycling type 1, **c** cycling type 2, and **d** isothermal annealed Vit-1 samples

Table 2 Values of Lasocka parameters and E_g for the as-cast- and thermal-treated Vit-1 samples determined using Moynihan equation and Kissinger equation

Sample	T_g assignment	Lasocka parameters		E_g/kJ mol^{-1}	
		A/°C	B	Moynihan Eq.	Kissinger Eq.
As-cast	$T_{g\text{-onset}}$	330.3	10.0	329.0	318.6
	$T_{g\text{-mid}}$	339.2	13.0	261.1	250.3
	$T_{g\text{-end}}$	348.3	15.9	215.3	204.2
Cycling type 1	$T_{g\text{-onset}}$	231.8	29.8	95.0	85.3
	$T_{g\text{-mid}}$	264.4	26.3	116.2	106.0
	$T_{g\text{-end}}$	297.0	22.8	141.9	131.4
Cycling type 2	$T_{g\text{-onset}}$	230.5	27.8	98.3	88.7
	$T_{g\text{-mid}}$	263.4	25.0	120.8	110.7
	$T_{g\text{-end}}$	296.3	22.2	145.4	134.9
Isothermal	$T_{g\text{-onset}}$	250.0	23.2	121.7	112.0
	$T_{g\text{-mid}}$	272.7	24.5	125.2	115.0
	$T_{g\text{-end}}$	296.1	25.5	129.3	118.8

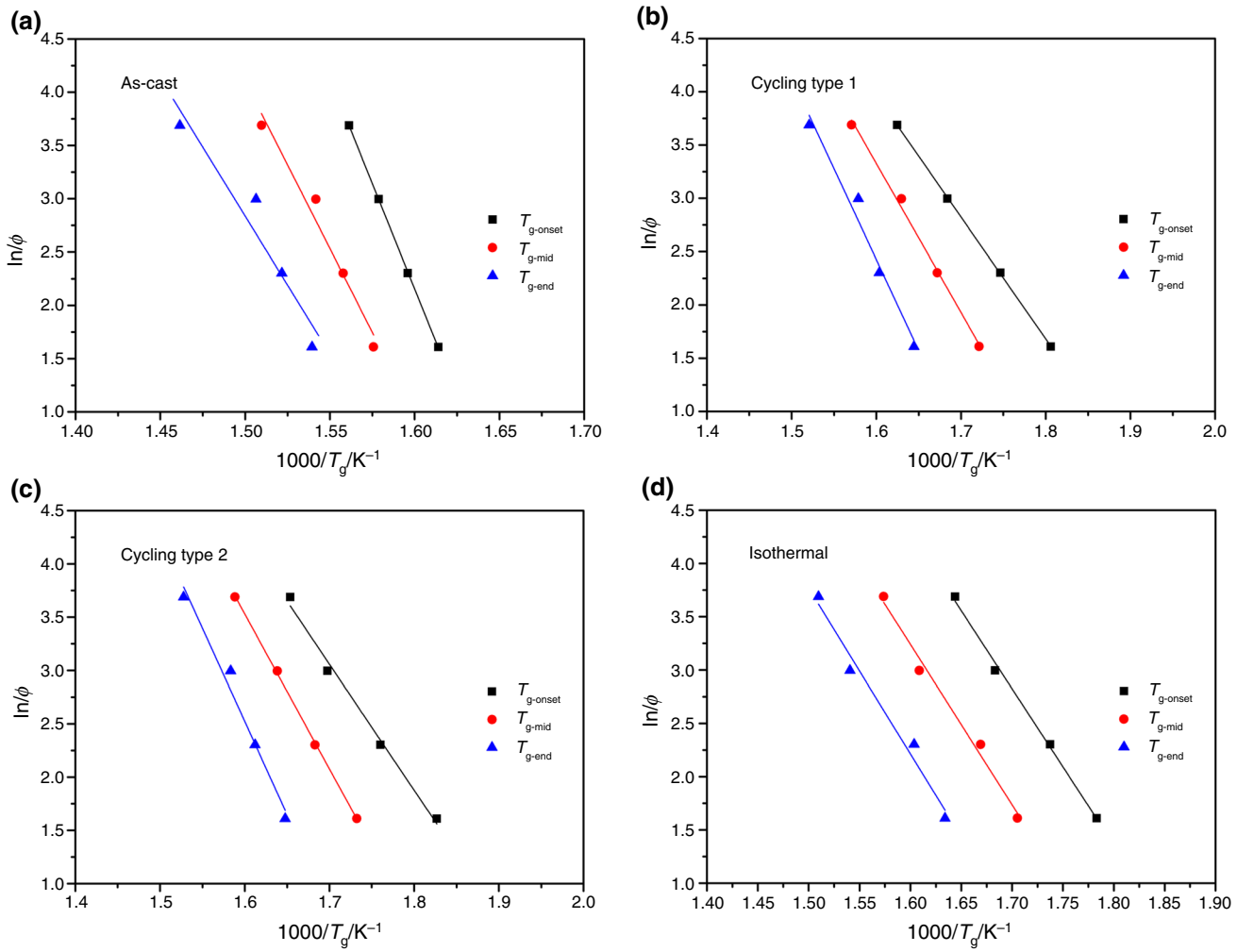

Fig. 5 Plots for the glass transition based on Moynihan equation: **a** as-cast, **b** cycling type 1, **c** cycling type 2, and **d** isothermal annealed Vit-1 samples

here T represents the onset and peak crystallization temperatures (e.g., T_x, $T_{p1,}$ and T_{p2}). E notes the corresponding apparent activation energy.

The related Kissinger and Ozawa plots corresponding to different methods for the first and second exothermic crystallization peaks of as-cast- and thermal-treated Vit-1 samples are shown in Figs. 7 and 8, respectively. Table 3 lists the values of E_x, $E_{p1,}$ and E_{p2} for the Vit-1 samples in different states. It is found that after thermal treatment, the activation energies for crystallization do not change as much as those of activation energies for glass transition. The thermal cycled samples possess slightly higher values of E_x, $E_{p1,}$ and E_{p2} than those of the isothermal annealed sample. Compared with the as-cast samples, the thermal cycled samples possess lower values of E_x. Regarding E_{p1} and E_{p2}, the values do not change a lot and no obvious change trend has been observed.

To further study the effect of thermal cycling on the crystallization kinetics of Vit-1 BMG, isothermal DSC tests have also been conducted. According to Table 1, the values of T_x for the studied four samples are similar. Thus, the annealing temperature for isothermal DSC was set to be 693 K, about 30 K lower than T_x measured at 20 K min^{-1}. As shown in Fig. 9, the isothermal DSC curve for the as-cast sample exhibits two crystallization peaks. The shape of the isothermal DSC curve for the cycling type 2 sample is similar as that of the as-cast sample. However, the shape of the cycling type 1 sample is obviously different from that of the as-cast sample, especially that the second crystallization peak becomes lower and broader. For the isothermal annealed sample, only one crystallization peak can be found from the corresponding isothermal DSC curve. The isothermal DSC results imply that the crystallization kinetics can be affected by thermal cycling. The relationship between x and annealing time t for the as-cast- and thermal-treated Vit-1 samples can be obtained (as shown in Fig. 10). To understand the crystallization mechanisms during the isothermal

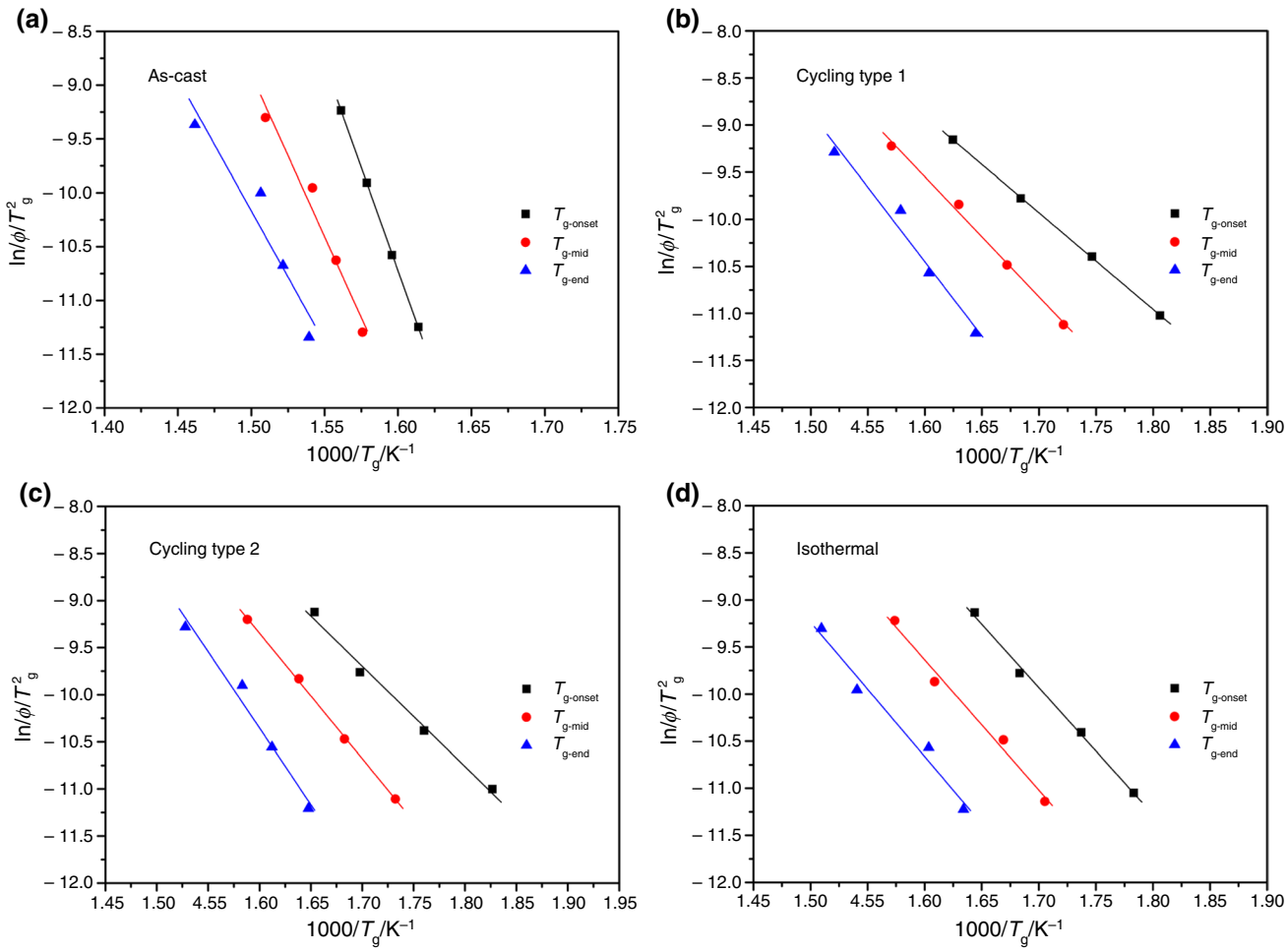

Fig. 6 Plots for the glass transition based on Kissinger equation: **a** as-cast, **b** cycling type 1, **c** cycling type 2, and **d** isothermal annealed Vit-1 samples

crystallization process in detail, we also studied the local Avrami exponent $n(x)$, which can be defined as [33]:

$$n(x) = \frac{\partial \ln[-\ln(1-x)]}{\partial \ln(t-\tau)} \tag{5}$$

where τ is the incubation time for crystallization.

Figure 11 shows the relationship between the local Avrami exponent and the crystallized volume fraction for the as-cast- and thermal-treated samples. For the as-cast and cycling type 2 sample, the local Avrami exponent first decreases from around 3 to less than 1 ($x = 0.57$), then increases to over 3, and decreases. Thus, the first crystallization event is fist dominated by a three-dimensional growth with a decreasing nucleation rate and then controlled by growth directly of preexisting nuclei. The second crystallization event is dominated mainly by a three-dimensional growth with an increasing nucleation rate. For the cycling type 1 sample, the crystallization mechanism of the first event is similar as that of as-cast and cycling type 2 sample. The difference is that the values of local Avrami exponent are obviously smaller, implying a lower nucleation rate. However, for the isothermal annealed sample, the local Avrami exponent decreases in the whole-crystallization process, from around 3 to around 1. The above experimental results indicate that thermal cycling may affect the crystallization kinetics of Vit-1 BMG and the cycling type plays an important role on this effect.

The effects of annealing on the glass transition and crystallization of BMGs have been studied in the past decades [34–36]. According to Chen's study [37], the isothermal annealing at temperatures lower than T_g can be classified into two types: sub-T_g annealing (T_g-100 K < $T_{annealing}$ < T_g) and sub–sub-Tg annealing (T_g-200 K < $T_{annealing}$ < T_g-100 K). During the structure relaxation process induced by sub-T_g annealing, the free volume annihilates and atomic structural rearrangement occurs in the local region [38]. The structure relaxation induced by sub-T_g annealing is mainly related

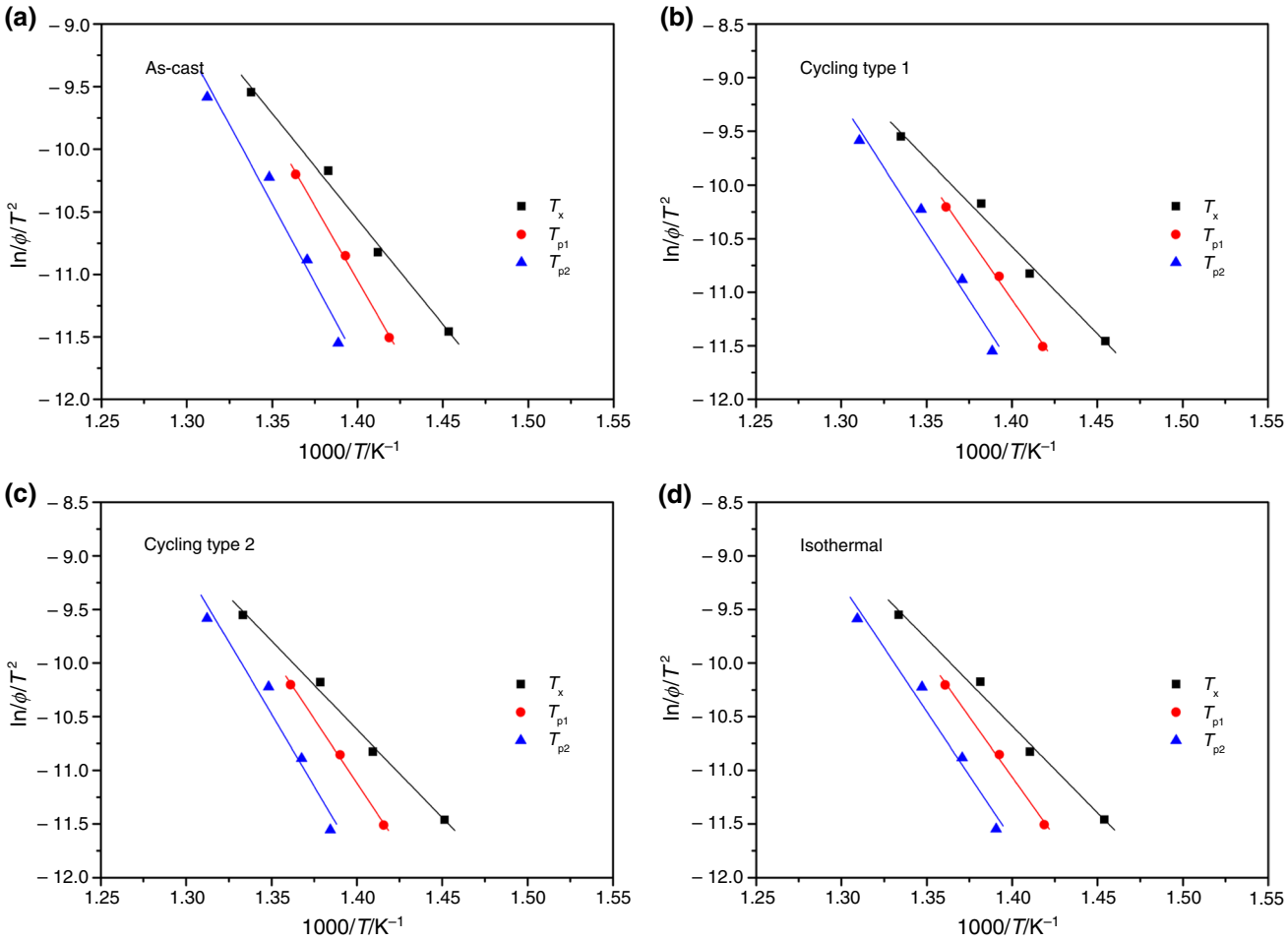

Fig. 7 Plots for the crystallization based on Kissinger equation: **a** as-cast, **b** cycling type 1, **c** cycling type 2, and **d** isothermal annealed Vit-1 samples

to α-relaxation and can be recovered once the BMG sample is heated to its supercooled liquid region. However, the mechanism of structure relaxation for sub–sub-T_g annealing is different from that of sub-T_g annealing. Sub–sub-T_g annealing always results in slow β-relaxation, which can be recovered during the cooling process [39]. Regarding the sub-T_g annealing, Wang et al. [23] found that for Vit 1 alloy, the values of E_g decrease and the values of E_x and E_p increase after sub-T_g annealing. This may be attributed to the local atomic structure and nuclei number formed during the sub-T_g annealing process. In our study, we found that after sub–sub-T_g annealing, the activation energies of glass transition also decrease obviously. However, the activation energies of crystallization decrease slightly after sub–sub-T_g annealing, and this result is different from that provided by Wang et al. [23]. Moreover, Venkataraman et al. [40] found that there is no qualitative modification in crystallization kinetics of Cu–Ti–Zr–Ni–Si BMG due to sub-T_g annealing because there is no difference in the n values for the as-prepared and annealed samples. According to Fig. 11, it is clear that sub–sub-T_g annealing changes the values of $n(x)$ for Vit-1 BMG, implying a different crystallization mechanism. In summary, the above results further confirm that the mechanisms of structure relaxation induced by thermal annealing at various temperatures may be quite different.

Martin et al. [41] studied the nanocrystallization of Vit-1 BMG using three-dimensional atom probe, transmission electron microscope, and small-angle X-ray scattering. They found that by isothermal annealing at a temperature slightly above T_g, nanoscale icosahedral phase (i-phase) precipitates first, followed by the formation of Be_2Zr and $CuZr_2$ phases. It has been confirmed that icosahedral clusters are the most stable short range ordered unit for densely packed liquid phase of multicomponent alloys, especially at relatively lower temperature [42]. For Vit-1 BMG, low temperature annealing can promote the formation of icosahedral clusters and stabilize some of these clusters to become effective nuclei for crystallization. However, as the structural relaxation induced by sub–sub-T_g can be recovered during the cooling process, the samples with different thermal cycling

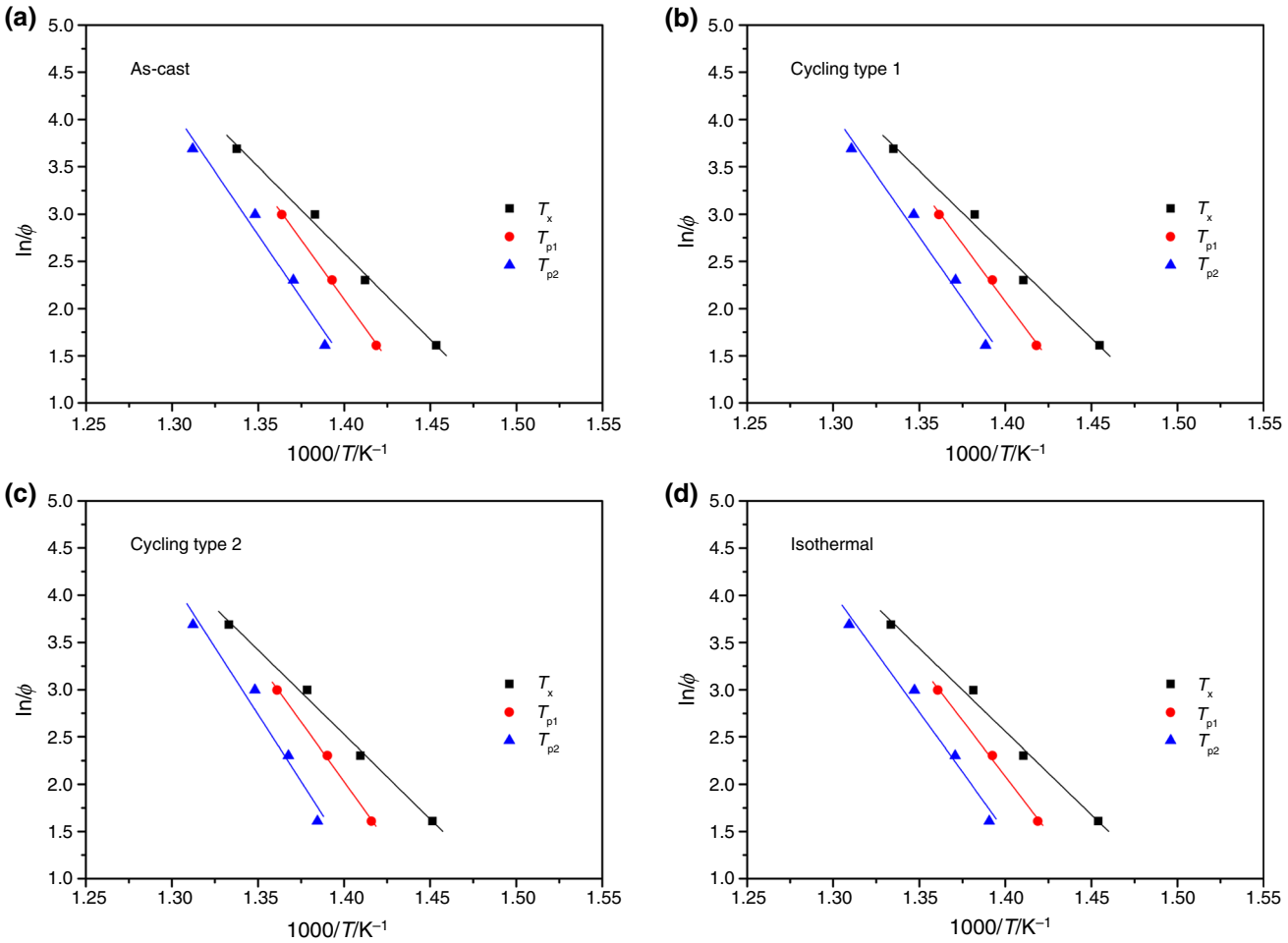

Fig. 8 Plots for the crystallization based on Ozawa equation: **a** as-cast, **b** cycling type 1, **c** cycling type 2, and **d** isothermal annealed Vit-1 samples

Table 3 Values of E_x, $E_{p1,}$ and E_{p2} for the as-cast- and thermal-treated Vit-1 samples determined using different equations

Sample	Method	E_x/kJ mol^{-1}	E_{p1}/kJ mol^{-1}	E_{p2}/kJ mol^{-1}
As-cast	Kissinger	140.1	197.5	210.1
	Ozawa	152.0	209.5	222.4
Cycling type 1	Kissinger	135.5	191.1	205.4
	Ozawa	147.4	203.1	217.7
Cycling type 2	Kissinger	136.8	198.3	223.5
	Ozawa	148.8	210.3	235.8
Isothermal	Kissinger	134.6	185.8	197.8
	Ozawa	146.5	197.7	210.1

treatment exhibit different glass transition and crystallization behaviors. Compared with cycling type 1, the total annealing time at 533 K is the same, but the number of cooling process for cycling type 2 is smaller, then the annealing effect can be maintained more. That is why the behaviors of glass transition and crystallization of cycling type 2 sample are

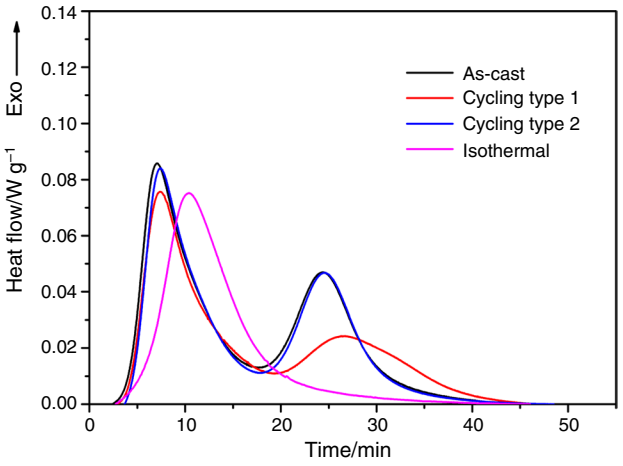

Fig. 9 Isothermal DSC curves for **a** as-cast, **b** cycling type 1, **c** cycling type 2, and **d** isothermal annealed Vit-1 samples

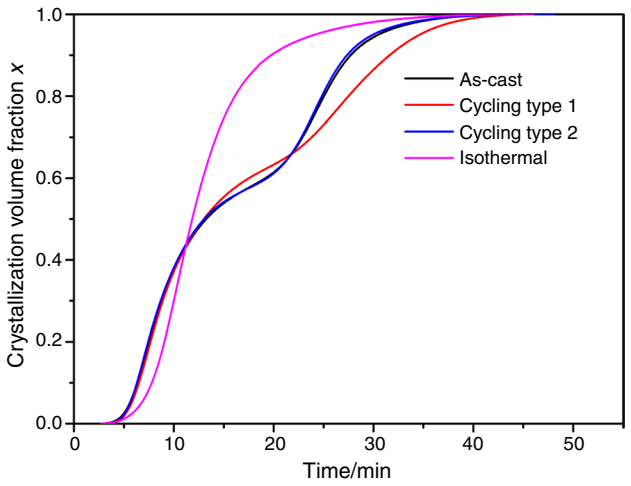

Fig. 10 Crystallized volume fraction x as a function of annealing time t for **a** as-cast, **b** cycling type 1, **c** cycling type 2, and **d** isothermal annealed Vit-1 samples

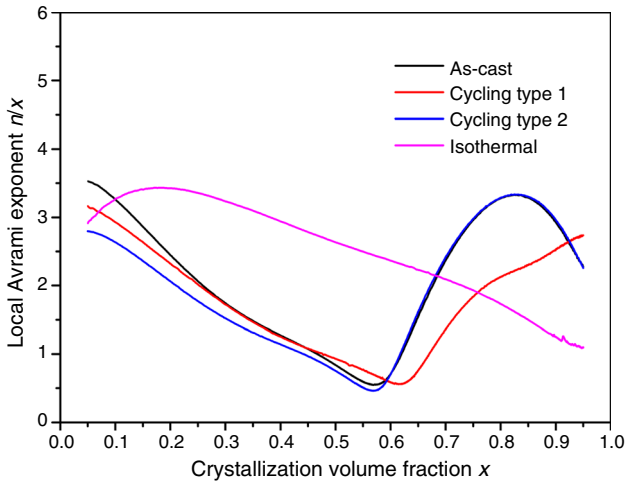

Fig. 11 Local Avrami exponent $n(x)$ as a function of the crystallized volume fraction x for **a** as-cast, **b** cycling type 1, **c** cycling type 2, and **d** isothermal annealed Vit-1 samples

more similar to those of the isothermal annealed sample. Our results show that the thermal cycling type can affect the kinetics of glass transition and crystallization of BMGs, and this may provide guidelines for the application of BMG parts in different areas such as aerospace engineering.

Conclusions

In this study, the thermal cycling effect on kinetics of glass transition and crystallization of a Vit-1 BMG has been studied by DSC. It is found that the kinetics nature of the glass transition for the Vit-1 BMG does not change after thermal cycling. The activation energies of glass transition decrease obviously, while the activation energies of crystallization decrease slightly. Thermal cycling type plays an important role on the crystallization kinetics of thermal cycled Vit-1 samples. On the premise of the same isothermal annealing temperature and total annealing time, decrease in the number of cycles and increase in the annealing time for one cycle are beneficial to keep the sub–sub-T_g annealing effect on the glass transition and crystallization of Vit-1 BMG.

Acknowledgements This work was financially supported by the National Natural Science Foundation of China (Grant No. 51601063), the National Science Foundation for Distinguished Young Scholars of China (Grant No. 51725504), the Research Fund of the State Key Laboratory of Advanced Design and Manufacturing for Vehicle Body (Grant No. 31715005), and Hubei Provincial Natural Science Foundation of China (Grant No. 2018CFB576). The authors are also grateful to the State Key Laboratory of Materials Processing and Die & Mould Technology and the Analytical and Testing Center, Huazhong University of Science and Technology, for technical assistance.

References

1. Jiang JZ, Hofmann D, Jarvis DJ, Fecht HJ. Low-density high-strength bulk metallic glasses and their composites: a review. Adv Eng Mater. 2015;17:761–80.
2. Wang WH, Dong C, Shek CH. Bulk metallic glasses. Mater Sci Eng R. 2004;44:45–89.
3. Yue Y, Wang R, Ma DQ, Tian JF, Zhang XY, Jing Q, Ma MZ, Liu RP. Fatigue behavior of a Zr-based bulk metallic glass under uniaxial tension–tension and three-point bending loading mode. Intermetallics. 2015;60:86–91.
4. Wang BP, Wang L, Wang S, Fan QB, Xue YF, Zhang HF, Fu HM. Mechanical response of Ti-based bulk metallic glass under plate-impact compression. Intermetallics. 2015;63:12–8.
5. Si JJ, Chen XH, Cai YH, Wu YD, Wang T, Hui XH. Corrosion behavior of Cr-based bulk metallic glasses in hydrochloric acid solutions. Corro Sci. 2016;107:123–32.
6. Maddala DR, Hebert RJ. Sliding wear behavior of $Fe_{50-x}Cr_{15}Mo_{14}C_{15}B_6Er_x$ ($x=0$, 1, 2 at.%) bulk metallic glass. Wear. 2012;294:246–56.
7. Huang Y, Zhang W, Fan H, Wang D, Sun J, Mi J. The effects of annealing on the microstructure and the dynamic mechanical strength of a ZrCuNiAl bulk metallic glass. Intermetallics. 2013;42:192–7.
8. Yoon KS, Lee M, Fleury E, Lee JC. Cryogenic temperature plasticity of a bulk amorphous alloy. Acta Mater. 2010;58:5295–304.
9. Gong X, Ma Y, Guo H, Gong S. Effect of thermal cycling on microstructure evolution and elements diffusion behavior near the interface of Ni/NiAl diffusion couple. J Alloys Compd. 2015;642:117–23.
10. Meng XL, Li H, Cai W, Hao SJ, Cui LS. Thermal cycling stability mechanism of $Ti_{50.5}Ni_{33.5}Cu_{11.5}Pd_{4.5}$ shape memory alloy with near-zero hysteresis. Scripta Mater. 2015;103:30–3.
11. Krooß P, Holzweissig MJ, Niendorf T, Somsen C, Schaper M, Chumlyakov YI, Maier HJ. Thermal cycling behavior of an aged FeNiCoAlTa single-crystal shape memory alloy. Scripta Mater. 2014;81:28–31.
12. Wang X, Shao Y, Gong P, Yao KF. Effect of thermal cycling on the mechanical properties of $Zr_{41}Ti_{14}Cu_{12.5}Ni_{10}Be_{22.5}$ alloy. Sci China Phys Mech Astron. 2012;55:2357–61.

13. Wang X, Shao Y, Gong P, Yao KF. The effect of simulated thermal cycling on thermal and mechanical stability of a Ti-based bulk metallic glass. J Alloys Compd. 2013;575:449–54.
14. Patel AT, Pratap A. Study of kinetics of glass transition of metallic glasses. J Therm Anal Calorim. 2012;110:567–71.
15. Wang SX, Quan SG, Dong C. Kinetic of glass transition of $Zr_{57.2}Al_{21.4}Ni_{21.4}$ bulk metallic glass. Thermochim Acta. 2012;532:92–5.
16. Guo N, Tang C, Wang J, Hu C, Zhou H. Kinetics of glass transition of $La_{65}Al_{20}Co_{15}$ metallic glass. J Alloys Compd. 2015;629:11–5.
17. Zhang B, Tang C, Xu W, Pan W, Wang J, Zhou H. Kinetics of glass transition of $Ce_{65}Al_{20}Co_{15}$ metallic glass. Mater Chem Phys. 2013;142:707–11.
18. Bai FX, Yao JH, Wang YX, Pan J, Li Y. Crystallization kinetics of an Au-based metallic glass upon ultrafast heating and cooling. Scripta Mater. 2017;132:58–62.
19. Yang M, Liu XJ, Ruan HH, Wu Y, Wang H, Lu ZP. High thermal stability and sluggish crystallization kinetics of high-entropy bulk metallic glasses. J Appl Phys. 2016;119:245112.
20. Gong P, Wang X, Yao KF. Effects of alloying elements on crystallization kinetics of Ti–Zr–Be bulk metallic glass. J Mater Sci. 2016;51:5321–9.
21. Sohn S, Jung Y, Xie Y, Osuji C, Schroers J, Cha JJ, Jung Y, Xie Y, Osuji C, Schroers J, Cha JJ. Nanoscale size effects in crystallization of metallic glass nanorods. Nat Commun. 2015;6:8157.
22. Wang X, Lee H, Yi S. Crystallization behavior of preannealed bulk amorphous alloy $Zr_{62}Al_8Ni_{13}Cu_{17}$. Mater Lett. 2006;60:935–8.
23. Zhuang YX, Wang WH. Effects of relaxation on glass transition and crystallization of ZrTiCuNiBe bulk metallic glass. J Appl Phys. 2000;87:8209–11.
24. Wang X, Gong P, Deng L, Jin J, Wang S, Li F. Sub-T_g annealing effect on the kinetics of glass transition and crystallization for a Ti-Zr-Be-Fe bulk metallic glass. J Non-Cryst Solids. 2017;473:132–40.
25. Peker A, Johnson WL. A highly processable metallic glass: $Zr_{41.2}Ti_{13.8}Cu_{12.5}Ni_{10.0}Be_{22.5}$. Appl Phys Lett. 1993;63:2342–4.
26. Lee SB, Kim NJ. Crystallisation kinetics of $Zr_{41.2}Ti_{13.8}Cu_{12.5}Ni_{10.0}Be_{22.5}$ BMG alloy during heating. Philoso Mag. 2005;85:139–52.
27. Cheng S, Wang C, Ma M, Shan D, Guo B. Non-isothermal crystallization kinetics of $Zr_{41.2}Ti_{13.8}Cu_{12.5}Ni_{10.0}Be_{22.5}$ amorphous alloy. Thermochim Acta. 2014;587:11–7.
28. Hays CC, Kim CP, Johnson WL. Large supercooled liquid region and phase separation in the Zr–Ti–Ni–Cu–Be bulk metallic glasses. Appli Phys Lett. 1999;75:1089–91.
29. Lasocka M. The effect of scanning rate on glass transition temperature of splat-cooled $Te_{85}Ge_{15}$. Mater Sci Eng. 1976;23:173–7.
30. Moynihan CT. Correlation between the width of the glass transition region and the temperature dependence of the viscosity of high-T_g glasses. J Am Ceram Soc. 1993;76:1081–7.
31. Kissinger HE. Reaction kinetics in differential thermal analysis. Anal Chem. 1957;29:1702–6.
32. Ozawa T. A new method of analyzing thermogravimetric data. J Bull Chem Soc Jpn. 1965;38:1881–6.
33. Calka A, Radliński AP. Decoupled bulk and surface crystallization in $Pd_{85}Si_{15}$ glassy metallic alloys: description of isothermal crystallization by a local value of the Avrami exponent. J Mater Res. 1988;3:59–66.
34. Frey M, Busch R, Possart W, Gallino I. On the thermodynamics, kinetics, and sub-Tg relaxations of Mg-based bulk metallic glasses. Acta Mater. 2018;155:117–27.
35. Liu C, Pineda E, Crespo D, Qiao J, Evenson Z, Ruta B. Sub-T_g relaxation times of the α process in metallic glasses. J Non Cryst Solids. 2017;471:322–7.
36. Dmowski W, Fan C, Morrison ML, Liaw PK, Egami T. Structural changes in bulk metallic glass after annealing below the glass-transition temperature. Mater Sci Eng A. 2007;471:125–9.
37. Chen HS. On mechanisms of structural relaxation in a $Pd_{48}Ni_{32}P_{20}$ glass. J Non-Cryst Solids. 1981;4:289–305.
38. Wang XD, Jiang JZ, Yi S. Reversible structural relaxation and crystallization of $Zr_{62}Al_8Ni_{13}Cu_{17}$ bulk metallic glass. J Non Cryst Solids. 2007;353:4157–61.
39. Mitrofanov YP, Afonin GV, Makarov AS, Kobelev NP, Khonik VA. A new understanding of the sub-T_g enthalpy relaxation in metallic glasses. Intermetallics. 2018;101:116–22.
40. Venkataraman S, Hermann H, Sordelet DJ, Eckert J. Influence of sub-T_g annealing on the crystallization kinetics of $Cu_{47}Ti_{33}Zr_{11}Ni_8Si_1$ metallic glass. J Appl Phys. 2007;104:066107.
41. Martin I, Ohkubo T, Ohnuma M, Deconihout B, Hono K. Nanocrystallization of $Zr_{41.2}Ti_{13.8}Cu_{12.5}Ni_{10.0}Be_{22.5}$ metallic glass. Acta Mater. 2004;52:4427–35.
42. Kelton KF, Lee GW, Gangopadhyay AK, Hyers RW, Rathz TJ, Rogers JR, Robinson MB, Robinson DS. First x-ray scattering studies on electrostatically levitated metallic liquids: demonstrated influence of local icosahedral order on the nucleation barrier. Phys Rev Lett. 2003;90:195504.